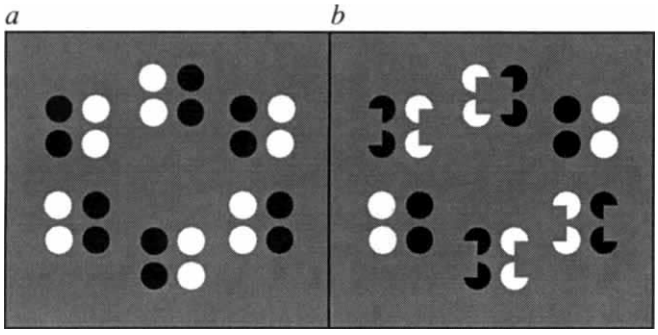

FIG. 4 Examples of the two successive displays within each trial of experiment 3, both to the same scale as in Fig. 2. *a*, The place-holder display, similar to experiments 1 and 2 except for the use of opposite-constrast circles against an intermediate grey background. Note that the side of black and of white circles is counterbalanced across clusters. Moreover, the arrangement of black and white circles was equally likely to be the opposite of that shown, and this was unpredictable across trials. *b*, The search display, which as before immediately replaced the place-holder display on its termination, and which again corresponded to the removal of 4 segments from each of a varied number of clusters (a set size of four candidate clusters is illustrated, but two or six were equally likely). Two of the inducers within the square target (shown at top) have common polarity. Note, however, that their arrangement is now shared with the nontarget clusters, so that the target is specified only by its arrangement of opposite-polarity inducers. Moreover, the side of black and white inducers for each cluster was both unpredictable across trials, and heterogeneous within trials, precluding any strategy of searching for a common-polarity subjective contour in a particular location. In all other respects, the method followed experiments 1 and 2. Experiment 4 was identical to experiment 3 except that different (substantially smaller) segments were removed from the place-holder displays to yield a search display that might contain an outline square target.

figure perception is thought to provide an anticamouflage device[21] which detects the non-accidental properties of otherwise hidden objects. Our parallel results make functional sense from this perspective, as such a device would be self-defeating if it required serial attentional scrutiny to detect camouflaged objects. Our findings do not, however, preclude a role for higher, possibly attentional, factors[2,4]. These may modulate the output of the parallel stages identified here so that, for instance, subjective figures are not seen when occlusion relations[4], or the completeness of familiar inducers[9], argue against the existence of an object under camouflage. □

Received 12 May; accepted 5 September 1994.

1. Peterhans, E. & von der Heydt, R. *Trends Neurosci.* **14,** 112–119 (1991).
2. Gregory, R. L. *Nature* **238,** 51–52 (1972).
3. Coren, S. *Psych. Rev.* **79,** 359–367 (1972).
4. Rock, I. & Anson, R. *Perception* **8,** 665–681 (1979).
5. Brigner, W. L. & Gallagher, M. B. *Percep. Motor Skills* **38,** 1047–1053 (1974).
6. Smith, A. T. & Over, R. *Nature* **257,** 581–582 (1977).
7. Grosof, D. H., Shapley, R. M. & Hawken, M. J. *Nature* **365,** 550–552 (1993).
8. von der Heydt, R., Peterhans, E. & Baumgarter, G. *Science* **224,** 1260–1262 (1984).
9. Kanizsa, G. *Rivista di Psicologia* **49,** 7–30 (1955).
10. Gurnsey, R., Humphrey, G. K. & Kapitan, P. *Percep. Psychophys.* **52,** 263–276 (1992).
11. Grabowecky, M. & Treisman, A. *Invest. Ophth. Vis. Sci:* suppl. **30,** 457 (1989).
12. Duncan, J. & Humphreys, G. W. *Psych. Rev.* **96,** 433–458 (1989).
13. Treisman, A. M. & Gelade, G. *Cog. Psych.* **12,** 97–136 (1980).
14. Enns, J. T. & Rensink, R. A. *Science* **247,** 721–723 (1990).
15. Townsend, J. T. *Percep. Psychophys.* **10,** 161–163 (1971).
16. Broadbent, D. E. in *Modelling Cognition* (ed. Morris, P.) 169–186 (Wiley, London, 1985).
17. Ginsburg, A. P. *Nature* **257,** 219–220 (1975).
18. Pradzny, K. *Percep. Psychophys.* **34,** 403–404 (1983).
19. De Valois, R. L. & De Valois, K. K. *Spatial Vision* (Oxford Univ. Press, Oxford, 1990).
20. Ginsburg, A. P. in *The Perception of Illusory Contours* (eds Petry, S. & Meyer, G. E.) 126 130 (Springer, New York, 1987).
21. Ramachandran, V. L. in *The Perception of Illusory Contours* (eds Petry, S. & Meyer, G. E.) 93–108 (Springer, New York, 1987).
22. Enns, J. T., Ochs, E. P. & Rensink, R. A. *Behavior Research Instruments & Computers* **22,** 118–122 (1990).
23. Warm, J. S., Dember, W. N., Padich, R. A., Beckner, J. & Jones, S. *Percep. Psychophys.* **39,** 219 (1986).

ACKNOWLEDGEMENTS. We thank C. Rorden and M. East. This work was supported by a grant from the Science and Engineering Research Council (UK).

Broad tuning for spatial frequency of neural mechanisms underlying visual perception of coherent motion

Yuede Yang & Randolph Blake

Department of Psychology, Vanderbilt University, Nashville, Tennessee 37240, USA

NEURAL events underlying perception of coherent motion are generally believed to be hierarchical[1,2]: information about local motion is registered by spatio-temporal coincidence detectors[3–5] whose outputs are cooperatively integrated at a subsequent stage[6,7]. There is disagreement, however, concerning the spatial scale of the neural filters underlying these operations. According to one class of models, motion registration is initially accomplished in parallel at multiple spatial scales[3–5], with filters tuned to lower spatial frequencies responsive to larger motion displacements than filters tuned to higher frequencies. According to another scheme, motion analysis involves a single, broadly tuned spatial filter, with optimal displacement dependent on spacing of local elements[8]. Here we use a masking procedure to measure the extent to which dynamic noise depicted at one spatial scale interferes with detection of coherent motion conveyed by image features at another spatial scale. Our results indicate that a single filter, broadly tuned for spatial frequency, is mediating detection of coherent motion. This finding dovetails with known physiological properties of neurons at an intermediate stage of motion processing.

Observers viewed two successive animation sequences each depicting a circular array of dots which were displaced from frame-to-frame of the sequence. In one sequence all dots were displaced upwards, yielding the perception of smooth, coherent motion, whereas in the other they were displaced in random directions, yielding incoherent motion; observers simply indicated which interval portrayed coherent motion, guessing if necessary. Superimposed on these two types of animation sequences (coherent and random motion) were dynamic noise dots that could be made sufficiently strong to destroy (mask) the perception of coherent motion, thus rendering the discrimination task impossible. Using spatial-frequency filtering techniques[9], the successive frames of the coherent motion sequence, the random motion sequence and the noise masks were band-pass filtered so that their spatial frequency content was only 0.4 octaves wide; the centre frequency of the noise was set independently of the centre frequency of the coherent and the random motion (Fig. 1). The root-mean-square (r.m.s.) contrast of the coherent and random motion sequences remained constant at 0.35; r.m.s. contrast of the mask was varied to find the value yielding 75% correct performance on this two-alternative, forced-choice task. In our initial experiment, dot displacement for the coherent motion sequence was approximately 1/2 cycle of the centre spatial frequency of the filtered sequence under test[10].

Viewed on their own without the addition of noise, these filtered animation sequences could be easily discriminated from uncorrelated sequences. Adding noise to this strong motion signal degraded the ability to detect coherent motion (Fig. 2), even when the spatial frequency content of the noise differed greatly from that of the coherent motion sequences. Applying statistical procedures[9], we found that all resulting masking tuning functions peaked at approximately the same value of 4 c deg^{-1} and that all had about the same full-width tuning of 2.4 octaves at the 3 dB roll-off point. These results implicate a single neural filter underlying coherent motion perception, a filter broadly tuned for spatial frequency. This conclusion is consistent with the single-channel model proposed by Morgan[8]. It is arguable, however, whether the filter implicated in our work operates at

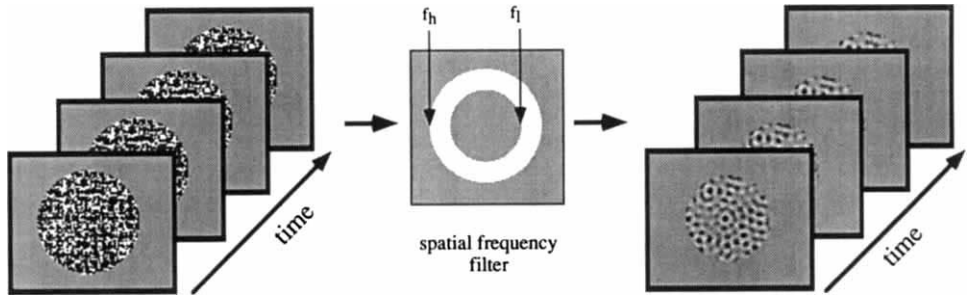

FIG. 1 Random-dot cinematograms (RDCs) were generated on a 19-inch radius grey-scale monitor (1152H × 882V pixel resolution; P104 phosphor) under control of a Macintosh II computer. Calibrated look-up tables were corrected for luminance nonlinearity. Each original unfiltered RDC consisted of ten successive frames (each of 84-ms duration), with each frame containing a circular area filled with 50% black (0.17 cdm^{-2}) and 50% white (74 cdm^{-2}) dots; the surrounding screen region was uniform grey (26 cdm^{-2}). Each dot was 2 × 2 pixels which, at the 0.8-m viewing distance, subtended 2.66 min arc × 2.66 min arc. The diameter of the circular, texture-filled region was 2.7 deg arc. Coherent motion was created by displacing all dots a specified number of pixels upwards. A schematic example of several frames of this complex (unfiltered) RDC is shown on the left. RDCs consisting entirely of random motion (no net movement in any given direction) were also created and constituted the incoherent motion and the noise masks. RDCs composed of narrow bands of spatial frequencies were created by filtering each of the ten frames of an RDC with a 0.4-octave isotropic filter (middle, with f_l and f_h referring to the low- and high-frequency cut-off). Filter size was 256 × 256 pixels, with highest spatial frequency 22 c deg^{-1} at the viewing distance of 0.8 m. A schematic example of several frames of the resulting RDCs are shown on the right. Temporal frequency remained constant (and speed varied) because frame-to-frame displacement varied inversely with centre spatial frequency. Incoherent motion and noise masks were comparably filtered.

the initial stage of motion registration as Morgan proposed, or at a subsequent stage at which local motion signals are integrated. It is noteworthy that the single, broadly tuned filter implicated in our work could register coherent motion signalled exclusively by high spatial frequencies, for others have shown that high spatial frequencies contribute to motion perception[11,12].

It could be argued that the 1/2-cycle displacement used in our animation sequences was not optimal for idealized motion-energy detectors[3-5], which are maximally responsive to 1/4-cycle displacements. We therefore repeated the masking experiment using dot displacements that were always 1/4 cycle of the centre spatial frequency of the sequence. Testing at three different centre spatial frequencies, we found that results were essentially

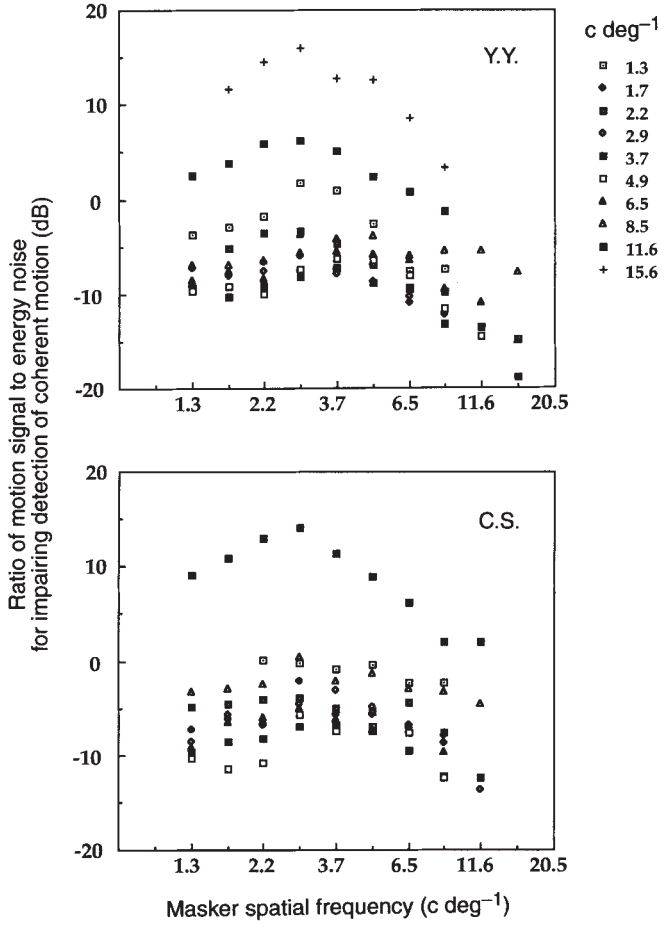

FIG. 2 Results from masking experiment. On each trial the observer viewed two successive animation sequences (each lasting 0.84 s and separated by a 1-s interval), one sequence being coherent upward motion and the other being incoherent random motion. The dots comprising both animation sequences were narrowly filtered with the same centre spatial frequency and bandwidth. The r.m.s. contrast of both types of animation sequence was held constant at 0.35. Following each trial, the observer judged which interval (first or second) contained the coherent motion sequence, with feedback. Narrowly filtered masking noise was added to both animation sequences, and the r.m.s. energy level of this masker varied from trial-to-trial within a range yielding seven signal-to-noise values (calculated as 20 × log (r.m.s.$_{signal}$/r.m.s.$_{masker}$), each differing by 1 dB. Over blocks of trials, the centre spatial frequency of the masker was varied relative to the centre spatial frequency of the motion sequences. Probit analysis was used to fit cumulative gaussian curves to the resulting psychometric functions, and the signal-to-noise value associated with the 75% point defined the masked threshold with this 2-interval forced-choice procedure. The graphs plot these threshold signal-to-noise values as a function of masker centre spatial frequency for two observers (one author and one naive). Each set of data points corresponds to a given centre spatial frequency of coherent motion, as denoted by the symbols shown to the right of the upper graph. Large signal-to-noise values indicate that relatively little noise energy noise was required to mask coherent motion. For these results, dot displacement was 1/2-cycle of the centre spatial frequency of the filtered coherent motion signal[10]. In a second experiment, essentially identical results were obtained using a 1/4-cycle displacement.

the same as those shown in Fig. 2, implying that the broadness of tuning is not attributable to the particular displacement used. The spatial frequency selectivity underlying the registration of coherent motion differs from that found for stereopsis[9], for detection of drifting gratings[13] and for integration of drifting cosine gratings into coherent plaids[14].

A third, ancillary experiment measured sensitivity to coherent motion by varying the percentage of dots moving coherently upwards; again the coherent motion sequences and the random-motion sequences were both narrowly filtered, but masking noise was not added to either sequence. Sensitivity to coherent motion varies with spatial frequency (Fig. 3), being highest near 4 c deg^{-1}, the same as the peak value implicated in our masking experiment.

Implications of our results are usefully portrayed in a space/time format[15]. For unfiltered animation sequences, upward coherent motion appears as diagonally oriented contours in the space/time domain (Fig. 4*A*). The two-dimensional Fourier power spectrum of this stimulus is defined by a streak of spatial and temporal frequency energy (Fig. 4*B*), whose orientation in the spectrum is proportional to motion speed. For coherent motion sequences that have been spatial frequency filtered, this streak is reduced to two small islands of spatio-temporal energy within the two-dimensional Fourier spectrum (Fig. 4*C*). The unfiltered noise masker, in comparison, consists of a disorganized, isotropic 'cloud' of dots in space/time (Fig. 4*D*) whose two-dimensional Fourier spectrum is likewise isotropic (Fig. 4*E*). When filtered, energy in the two-dimensional spectrum of the noise is broadly distributed in temporal frequency but narrowly distributed in spatial frequency (Fig. 4*F*). Presumably, masking (impaired perception of coherent motion by addition of dynamic noise) involves obliteration of the 'island' of spatio-temporal energy associated with coherent motion (Fig. 4*C*). Our results show that this destructive interference occurs even when signal and noise occupy different regions of the two-dimensional energy spectra. In other words, the filters underlying detection of coherent motion have relatively broad spectral bandwidths. This makes computational sense, for broad spatial frequency tuning implements integration of local motion signals over space, a requisite for perception of coherent motion[11,16]. Exactly where these broadly tuned filters fit into the energing picture of multiple motion pathways[17,18] remains to be determined. As for the actual neural bases of the mechanism isolated and studied here, the broad spatial frequency tuning for coherent motion is a property

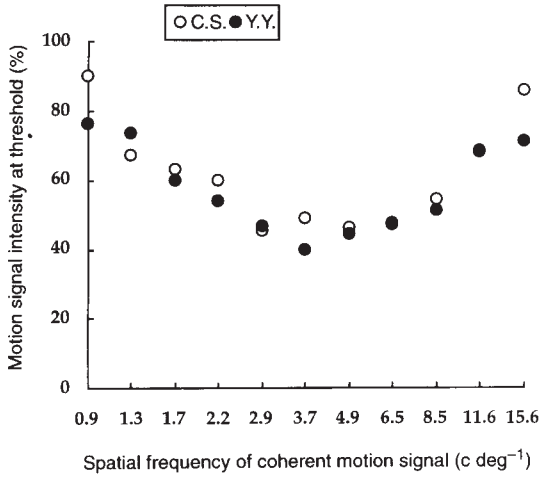

FIG. 3 To assess detectability of coherent motion signalled at different spatial scales, the percentage of RDC dots moving upwards was varied to determine the minimum signal strength supporting 75%-correct detection of coherent motion of filtered (but unmasked) RDCs. On each trial in a 2-interval forced-choice experiment, one interval displayed uncorrelated motion (0% coherent motion signal) and the other displayed coherent motion whose signal strength (percentage of upward-moving dots) varied over trials; the observer indicated which interval contained coherent motion, with feedback given. Signal dots were displayed by an amount equal to ~1/2-cycle of the centre spatial frequency[10]. Resulting thresholds (determined by probit analysis) for two observers reveal that sensitivity for coherent motion is greatest near 4 c deg $^{-1}$. Coherence thresholds here are somewhat higher than those reported previously for unfiltered RDCs[16], probably because the much higher dot density in our animation sequences creates more potential false matches.

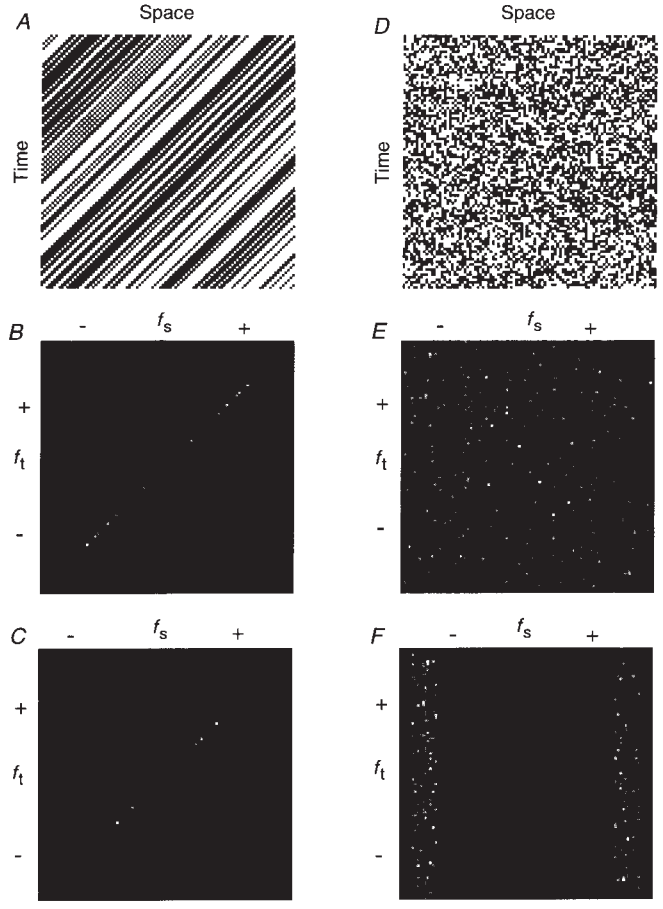

FIG. 4 Space/time portrayals of coherent motion and masking noise, together with their two-dimensional (2-D) Fourier power spectra. *A*, Plot showing successive vertical positions of unfiltered dots (50% black/50% white) moving coherently upwards in fixed displacements from frame to frame at a constant speed. In this plot the bottom row of dots represents dot positions at time t_1 and successively higher rows denote the vertical positions of those dots at times $t_2 \ldots t_n$. Because all dots move coherently upward, any given dot's position does not change horizontally over time. *B*, 2-D Fourier power spectra of the event depicted in *A*. Because dots were unfiltered, energy is distributed broadly in spatial frequency and in temporal frequency. *C*, 2-D Fourier power spectra of coherent motion of spatially filtered dots. Energy is concentrated in small 'islands' of the spectra, corresponding to the centre frequency of the bandpass of the filter. Limiting spatial frequency content also limits temporal frequency. *D*, Space-time plot for dynamic masking noise, where individual dots are simply replotted from frame-to-frame; perceptually, this event looks like random snow on a detuned television. *E*, 2-D Fourier power spectra of the unfiltered masking noise. *F*, 2-D Fourier power spectra of spatially filtered masking noise. Energy is concentrated in spatial frequency but widely distributed in temporal frequency.

more characteristic of neurons in the middle temporal visual area, not neurons in area V1[19]. □

Received 15 July; accepted 2 September 1994.

1. Movshon, A. in *Images and Understanding* (eds Barlow, H., Blakemore, C. & Weston-Smith, M.) (Cambridge University Press, Cambridge, 1990).
2. Braddick, O. *Trends Neurosci.* **16,** 263–268 (1993).
3. Adelson, E. H. & Bergen, J. R. *J. opt. Soc. Am.* A**2,** 284–299 (1985).
4. Van Santen, J. P. H. & Sperling, G. *J. opt. Soc. Am.* A**1,** 451–473 (1984).
5. Watson, A. B. *et al. J. opt. Soc. Am.* A**3,** 300–307 (1986).
6. Chang, J. J. & Julesz, B. *Vision Res.* **24,** 1781–1788 (1984).
7. Nawrot, M. & Sekuler, R. *Vision Res.* **30,** 1439–1451 (1990).
8. Morgan, M. J. *Nature* **355,** 344–346 (1992).
9. Yang, Y. & Blake, R. *Vision Res.* **31,** 1177–1190 (1991).
10. Cleary, R. & Braddick, O. *Vision Res.* **30,** 303–316 (1990).
11. Smith, A. T. *et al. Vision. Res.* **34,** 2425–2430 (1994).
12. van de Grind, W. A. *et al. Expl. Brain Res.* **91,** 135–150 (1992).
13. Anderson, S. J. & Burr, D. C. *Vision Res.* **13,** 1147–1154 (1985).
14. Adelson, E. H. & Movshon, J. A. *Nature* **300,** 523–525 (1982).
15. Adelson, E. H. *Opt. Photon. News* **2,** 24–30 (1991).
16. Williams, D. W. & Sekuler, R. *Vision Res.* **24,** 55–62 (1984).
17. Werkhoven, P., Sperling, G. & Chubb, C. *Vision Res.* **33,** 463–485 (1993).
18. Wilson, H. R. & Kim, J. *Vision Res.* **34,** 1835–1842 (1994).
19. Britten, K. H. *et al. Vis. Neurosci.* **10,** 1157–1169 (1993).

ACKNOWLEDGEMENTS. Supported by a research grant (R.B.) and a Vision Core grant from the NIH.

Krox-20 controls myelination in the peripheral nervous system

Piotr Topilko*, Sylvie Schneider-Maunoury*, Giovanni Levi*†, Anne Baron-Van Evercooren‡, Amina Ben Younes Chennoufi‡, Tania Seitanidou*, Charles Babinet§ & Patrick Charnay*

* Unité 368 de l'Institut National de la Santé et de la Recherche Médicale, Ecole Normale Supérieure, 46 rue d'Ulm, 75230 Paris Cedex 05, France
† Advanced Biotechnology Center, Viale Benedetto XV n°10, 16132 Genova, Italy
‡ Unité 134 de l'Institut National de la Santé et de la Recherche Médicale, Hôpital de la Salpêtrière, 75651 Paris Cedex 13, France
§ Unité de Recherche Associée 361 du Centre National de la Recherche Scientifique, Institut Pasteur, 75724 Paris Cedex 15, France

THE molecular mechanisms controlling the process of myelination by Schwann cells remain elusive, despite recent progress in the identification and characterization of genes encoding myelin components (reviewed in ref. 1). We have created a null allele in the mouse *Krox-20* gene, which encodes a zinc-finger transcription factor[2,3], by in-frame insertion of the *Escherichia coli lacZ* gene, and have shown that hindbrain segmentation is affected in *Krox-20*$^{-/-}$ embryos[4]. We demonstrate here that *Krox-20* is also activated in Schwann cells before the onset of myelination and that its disruption blocks Schwann cells at an early stage in their differentiation, thus preventing myelination in the peripheral nervous system. In *Krox-20*$^{-/-}$ mice, Schwann cells wrap their cytoplasmic processes only one and a half turns around the axon, and although they express the early myelin marker, myelin-associated glycoprotein[5], late myelin gene products are absent, including those for protein zero[6] and myelin basic protein[7]. Therefore *Krox-20* is likely to control a set of genes required for completion of myelination in the peripheral nervous system.

In late embryos, the *Krox-20/lacZ* chimaeric gene is expressed in a complex pattern revealing a number of potential sites of *Krox-20* expression (P.T. *et al.*, manuscript in preparation), including part of the peripheral nervous system (PNS). Between 10 and 15 days after birth, surviving *Krox-20*$^{-/-}$ mutant mice tremble[4], suggesting a possible phenotypic effect of the mutation on the PNS, so we analysed *Krox-20/lacZ* expression in the PNS in greater detail. No qualitative differences in β-galactosidase activity were observed between heterozygotes and homozygotes during embryogenesis, although the intensity of the labelling was stronger in homozygotes (data not shown). In the PNS, β-galactosidase is first detected in boundary cap cells that surround nerve exit points from the central nervous system (CNS) around 10.5 days post-coitum (d.p.c.)[4,8]. Up to 14.5 d.p.c., PNS expression is confined to the motor and sensory roots of cranial and spinal nerves, with no labelling of the ganglia or of more distal parts of the fibres (Fig. 1*a*), with the exception of the XIth cranial nerve which is labelled along its path adjacent to the CNS[4]. A major transition occurs around 15.5 d.p.c., when *Krox-20/lacZ* is activated along the entire length of peripheral nerves (Fig. 1*b*, *c*). However, no β-galactosidase is detected within cranial and dorsal root ganglia or in the sympathetic system (Fig. 1 and data not shown). This expression persists during the entire life of the animal. Myelination in the PNS occurs during the first 2 weeks after birth, and in heterozygous animals, β-galactosidase activity is detected in the cytoplasm of myelinating Schwann cells (Fig. 1*d*). *In situ* hybridizations on sections from wild-type animals confirmed that *Krox-20/lacZ* expression in peripheral nerves reflects normal expression of *Krox-20* (Fig. 1*e*). This distribution strongly suggests that expression in the PNS is restricted to myelinating Schwann cells and putative Schwann cell precursors[9] and, indeed, purified Schwann cells from newborn sciatic nerves express *Krox-20* (P. Murphy *et al.*, manuscript in preparation).

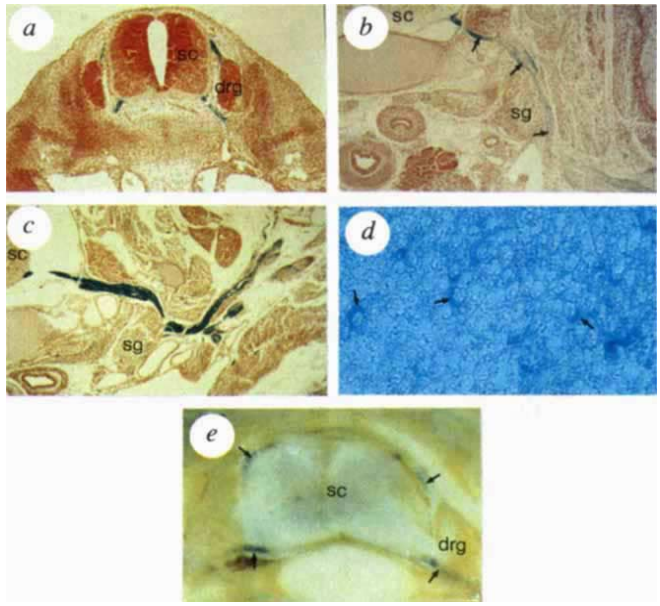

FIG. 1 Expression of *Krox-20* in the developing PNS. *a–d*, Staining for β-galactosidase activity: *a*, transverse section through the trunk of an 11.5-d.p.c. *Krox-20*$^{-/-}$ embryo. Note that *Krox-20–lacZ* expression is restricted to the motor and sensory roots of the nerve; *b*, *c*, transverse sections through 15.5- and 17.5-d.p.c. *Krox-20*$^{-/-}$ embryos, respectively. At these stages the spinal nerves (arrows) are stained along most of their length. Note the increase in the intensity of staining in the older embryo; *d*, cross-section of a sciatic nerve from a P10 heterozygous mutant mouse. The cytoplasms of Schwann cells (arrows) but not the axons are labelled. *e*, *In situ* hybridization of a transverse section through the trunk of a 15.5-d.p.c. embryo with a *Krox-20* cDNA probe[8] labelled with digoxygenin. Note the labelling along both the motor and sensory roots (arrows). sc, Spinal cord; drg, dorsal root ganglion; sg, sympathetic ganglion. For β-galactosidase revelation, embryos and nerves were processed as described[4]. *In situ* hybridization of 150-μm vibratome-cut embryo sections were as described[4]. Magnification in *a*, *b*, *c*, *e*: ×12; in *d*, ×120.